

## THE PROFILE OF AN EMISSION LINE FROM RELATIVISTIC OUTFLOWS AROUND A BLACK HOLE

JIAN-MIN WANG<sup>1,2</sup>, YOU-YUAN ZHOU<sup>2,3,5</sup>, YE-FEI YUAN<sup>3,5</sup>, XINWU CAO<sup>4,5</sup>, AND MEI WU<sup>1</sup>

*The Astrophysical Journal*, 544, No.1, Nov. 20, 2000

### ABSTRACT

Recent observations show strong evidence for the presence of Doppler-shifted emission lines in the spectrum of both black hole candidates and active galactic nuclei. These lines are likely to originate from relativistic outflows (or jets) in the vicinity of the central black hole. Consequently, the profile of such a line should be distorted by strong gravitational effects near the black hole, as well as special relativistic effects. In this paper, we present results from a detailed study on how each process affects the observed line profile. We found that the profile is sensitive to the intrinsic properties of the jets (Lorentz factor, velocity profile, and emissivity law), as well as to the spin of the black hole and the viewing angle (with respect to the axis of the jets). More specifically, in the case of approaching jets, an intrinsically narrow line (blue-shifted) is seen as simply broadened at small viewing angles, but it shows a doubly peaked profile at large viewing angles for extreme Kerr black holes (due to the combination of gravitational focusing and Doppler effects); the profile is always singly peaked for Schwarzschild black holes. For receding jets, however, the line profile becomes quite complicated owing to complicated photon trajectories. To facilitate comparison with observations, we searched a large parameter space to derive representative line profiles. We show the results and discuss how to use emission lines as a potential tool for probing the inner region of a black hole jet system.

*Subject headings:* black hole physics – line: profile – relativity

### 1. INTRODUCTION

Recently, the *ASCA* observations of two radio-loud quasars, PKS 0637-752 (at  $z=0.654$ ) and PKS 2149-306 (at  $z=2.345$ ), revealed evidence for the presence of Doppler-shifted emission lines in the X-ray spectra of these objects (Yaqoob et al. 1998, 1999). For PKS 0637-752, the line observed at  $\sim 1$  keV (or  $\sim 1.6$  keV in the rest-frame of the source) was interpreted as the blue-shifted OVII line; for PKS 2149-306, the line observed at  $\sim 5.1$  keV (or  $\sim 17$  keV in the rest-frame of the source) was thought to be the blue-shifted iron K emission line. If the interpretation is valid, the inferred Doppler-shift of the lines would be quite similar for both quasars; such emission lines would be likely to originate in the relativistic jets (Yaqoob et al. 1999). This is in contrast to the case of Seyfert galaxy MCG 6-30-15, where iron  $K\alpha$  line is detected and its profile has a strong wing toward *low* energies (Tanaka et al 1995). Such a profile is characteristic of emission lines from the inner region of the accretion disk (Fabian et al. 1989, 1995). Although the disk origin of the line seems secure for MCG 6-15-30 (see Misra 1999 and Reynolds 1999 for more evidence), the observed iron  $K\alpha$  line is too broader to be accounted for by this scenario for 3C 120 and 3C 382 (both are radio-loud; Reynolds 1997). Perhaps, the latter can also be attributed to relativistic jets.

For stellar-mass black hole candidates, Margon et al (1979) found the large, periodic Doppler drift in the optical lines of SS 433. This has been explained remarkably well

by a kinematic model (Fabian & Rees 1979) which invokes two processing jets with velocity of 0.26 light speed (see review by Margon 1984). More recently, Cui et al. (1999) reported the detection of two emission lines at  $\sim 5.7$  keV and 7.7 keV in black hole candidate 4U 1630-47. They proposed that the lines might arise from a single emission line due to highly ionized ions of Fe that is Doppler red- and blue-shifted either in a Keplerian accretion disk or in a bi-polar outflow (or even both). The quality of the data does not allow them to distinguish between the two possibilities.

In this paper, we make an attempt to deriving the profile of an emission line from relativistic jets around a black hole, taking into account of both general and special relativistic effects. We present the predictions of the model and discuss potential applications of the results.

### 2. THE MODEL

Since we are primarily interested in studying relativistic effects on the profile of emission lines, we chose to neglect the details of the outflow (or jet) dynamics and the emission processes of the lines. In the model, a jet is treated as a pencil beam along the spin axis of a Kerr black hole. We consider a twin-jet scenario where two jets run in the opposite direction away from the black hole. Recent numerical simulations of jets or outflows from an accretion disk show that the jets may form very close to the black hole (Koide et al 1999). Since the accretion disk cannot

<sup>1</sup>Laboratory for Cosmic Ray and High Energy Astrophysics, Institute of High Energy Physics, CAS, Beijing 100039, P.R. China, wangjm@astrosv1.ihep.ac.cn

<sup>2</sup>CAS-PKU Beijing Astrophysical Center, Beijing 100871, P. R. China

<sup>3</sup>Center for Astrophysics, University of Science and Technology of China, Hefei 230026, P.R. China, yzzhou, yfyuan@ustc.edu.cn

<sup>4</sup>Shanghai Observatory, The Chinese Academy of Sciences, Shanghai 200019, P. R. China, cxw@center.shao.ac.cn

<sup>5</sup>National Astronomical Observatories, The Chinese Academy of Sciences, P.R. China

extend toward the black hole beyond the marginally stable orbit (of radius  $r_{\text{ms}}$ ), for simplicity, we assume that the jets start at a distance,  $r_{\text{ms}}$ , away from the black hole.

A Kerr black hole is fully characterized by its mass ( $M$ ) and dimensionless specific angular momentum ( $a \in [0, 1]$ ). The spacetime around such a black hole is described by a metric that is appropriate to a stationary axial symmetry case in the usual form (Misner, Thorne & Wheeler 1973). We adopt the Boyer-Lindquist coordinates and natural units in which  $G = c = M = 1$ , where  $G$  and  $c$  are the gravitational constant and the speed of light, respectively. The propagation of photons can be described by the distribution of photon in phase space defined as  $N(x_\mu, k_\mu) = dn/d^3x d^3k$ , where  $x_\mu$  and  $k_\mu$  are space and momentum coordinates, respectively.  $N(x_\mu, k_\mu)$  satisfies the general form of Liouville's theorem,  $dN(x_\mu, k_\mu)/d\lambda = 0$ , which conserves the total number of photons along a trajectory (Thorne 1967, Ames & Thorne 1968, Gerlach 1971). The Liouville's equation can be rewritten as

$$k^\alpha \frac{\partial N}{\partial x^\alpha} - \frac{1}{2} \frac{\partial g^{\sigma\nu}}{\partial x^\alpha} k_\sigma k_\nu \frac{\partial N}{\partial k_\alpha} = 0. \quad (1)$$

$N(x_\mu, k_\mu)$  is determined by three constants of motion, total energy  $k_0$ , angular momentum component along the symmetry axis  $k_\phi$ , and Carter's constant  $Q$  (Carter 1968), as well as by the initial photon locations. The solution to eq.(1) is given by

$$N(x_\mu, k_\mu) = \varepsilon(r) \delta(u^\mu k_\mu - \epsilon_0), \quad (2)$$

where  $\varepsilon(r)$  is the emissivity function of the jets (at energy  $\epsilon_0$ ) and  $u^\mu$  the four-velocity. Note that we take the intrinsic profile of the emission line to be a  $\delta$  function, although it is probably of a Lorentz shape in reality. A photon trajectory is determined by two dimensionless variables:  $p = -k_\phi/k_0$  and  $q = Q^{1/2}/k_0$ .

For the approaching jet, we have

$$N(x_\mu, k_\mu) = \varepsilon(r) \delta(k_0 x - \epsilon_0), \quad (3)$$

where  $x$  is defined by

$$x = u^t - u^r \left( \frac{R^{1/2}}{\Delta} \right). \quad (4)$$

In this case, the equation of null geodesic can be simplified to (Carter 1968, Bardeen et al 1972)

$$\int_{r_j}^{\infty} \frac{dr}{R^{1/2}} = \frac{F(k, \theta_{\text{obs}})}{\sqrt{q^2 + a^2}}, \quad (5)$$

where

$$R = \frac{V_r}{E^2} = (r^2 + a^2)^2 - \Delta(a^2 + q^2), \quad (6)$$

with  $\Delta = r^2 + a^2 - 2r$ , and  $F(k, \theta_{\text{obs}})$  is the usual elliptical integral defined as  $F(k, \theta_{\text{obs}}) = \int_0^{\theta_{\text{obs}}} d\phi / (1 - k^2 \sin^2 \phi)^{1/2}$  with  $k^2 = a^2 / (a^2 + q^2)$ . The left-hand side of eq.(5) can be expressed analytically by elliptical integrals (Cadez, Fanton & Calvani 1998). We note that  $k_\phi = 0$  for our case because the jets are assumed to coincide with the spin axis of the black hole. The equation of motion gives  $k_r = -k_0 R^{1/2} / \Delta$  (Bardeen et al. 1972).

We investigate two cases: (1) jets of constant Lorentz factor ( $\Gamma_0$ ) and (2) jets of an accelerating velocity profile

$$\Gamma = 1 + (\Gamma_0 - 1) \tanh[\gamma(r - r_{\text{ms}})]. \quad (7)$$

The parameter  $\gamma$  sets a scale for jet acceleration; the Lorentz factor of the jets approaches the final value ( $\Gamma_0$ ) about  $3/\gamma$ . The symmetry of the problem requires  $u^\theta = 0$  and  $u^\phi = 0$ , so we have

$$u^t = \frac{1}{\sqrt{1 - (v^r)^2}} \frac{1}{\sqrt{-g_{tt}}}; \quad u^r = \frac{1}{\sqrt{g_{rr}}} \frac{v^r}{\sqrt{1 - (v^r)^2}}, \quad (8)$$

where  $v^r$  is the physical radial velocity of the jets,  $v^r = \Gamma^{-1} \sqrt{\Gamma^2 - 1}$ , and the metric parameters  $g_{tt} = 2r/\Sigma - 1$  and  $g_{rr} = \Sigma/\Delta$  are given by the Kerr solutions with  $\Sigma = r^2 + a^2 \cos^2 \theta$  and  $\Delta = r^2 - 2r + a^2$ . Finally, we assume a simple power law for the emissivity of the jets, i.e.,  $\varepsilon(r) = Kr^{-m}$ , which may or may not be reasonable for real systems.

The observed profile of an emission line from the approaching jet can then be obtained by integrating over the entire length of the jet,

$$I(\epsilon) = K \epsilon^3 \int_{r_1}^{r_2} dr \left( \frac{d\beta}{dr} \right) r^{-m} \delta(\epsilon x - \epsilon_0), \quad (9)$$

where  $\beta = (q^2 + a^2 \cos^2 \theta_{\text{obs}})^{1/2}$  is the impact parameter, indicating the apparent displacement parallel to the axis of symmetry in the sense of the angular momentum of the black hole (Cunningham & Bardeen 1973);  $\epsilon$  is the energy of photons as measured by a distant observer; and  $\theta_{\text{obs}}$  is the viewing angle with respect to the axis of the jet. We have

$$I(\epsilon_*, \theta_{\text{obs}}) = \left( \frac{K}{\epsilon_0} \right) \left( \frac{d\beta}{dr} \right) \frac{\epsilon_*^2 r^{-m}}{(U_1 + U_2 + U_3)} \Big|_{x=1/\epsilon_*}. \quad (10)$$

where  $\epsilon_* = \epsilon/\epsilon_0$ ,

$$U_1 = \left( \frac{d\Gamma}{dr} \right) \frac{1}{\sqrt{-g_{tt}}} + \frac{\Gamma}{\Sigma^2} (a^2 - r^2), \quad (11)$$

$$U_2 = \frac{u^r}{\Delta^2 R^{1/2}} (\Delta R_1 - R \Delta_1), \quad (12)$$

and

$$U_3 = \left( \frac{R^{1/2}}{\Delta} \right) \left( \frac{du^r}{dr} \right), \quad (13)$$

with

$$R_1 = 4r^3 + 2(r+1)a^2 - 2\Delta \left( \frac{dr}{dq} \right)^{-1} - q^2 \Delta_1, \quad \Delta_1 = 2(r-1). \quad (14)$$

We caution that care must be taken in the derivation since  $x$  may be a double-valued function.

For the receding jet, there are two types of photon trajectories: (1) there are no turning points in  $\theta$ -direction (but possibly in  $r$ -direction), and (2) there is a turning point in  $\theta$ -direction. For Case 1, the trajectory equation becomes

$$\pm \int_{r_0}^{r_j} \frac{dr}{R^{1/2}} + \int_{r_0}^{\infty} \frac{dr}{R^{1/2}} = \frac{1}{\sqrt{q^2 + a^2}} \int_{\theta_{\text{obs}}}^{\pi} \frac{d\phi}{(1 - k^2 \sin^2 \phi)^{1/2}}, \quad (15)$$

where  $r_0$  is the turning point, which can be determined by setting  $R = 0$  for a given  $q$ . For Case 2, the trajectory equation is

$$\pm \int_{r_0}^{r_j} \frac{dr}{R^{1/2}} + \int_{r_0}^{\infty} \frac{dr}{R^{1/2}} = \frac{1}{\sqrt{q^2 + a^2}} \left[ \int_0^{\pi} \frac{d\phi}{(1 - k^2 \sin^2 \phi)^{1/2}} \pm \int_{\theta_{\text{obs}}}^{\pi} \frac{d\phi}{(1 - k^2 \sin^2 \phi)^{1/2}} \right], \quad (16)$$

where the  $\theta$ -turning point is at  $\theta = 0$  for photons with zero angular momentum.

Also for the receding jet, after the turning point in  $r$  direction,  $x$  should be replaced by

$$x = u^t + u^r \left( \frac{R^{1/2}}{\Delta} \right), \quad (17)$$

for eq. (10). The line profile can then be derived following the same procedure as for the approaching jet.

### 3. NUMERICAL RESULTS

To summarize, there are five free parameters in the model:  $m$ ,  $\theta_{\text{obs}}$ ,  $\gamma$ ,  $\Gamma_0$ , and  $a$ . In our calculations, we allowed  $m$  to vary in the range of 0.1 to 3,  $\theta_{\text{obs}}$  in the range of  $5^\circ$  to  $75^\circ$ , and  $\gamma$  in the range of 0.01 to 1; we fixed  $\Gamma_0$  at 5 and examined two extreme cases for black hole spin, 0 and 0.998.

For better understanding the numerical results, we began by deriving approximate analytic solutions to the photon trajectory equations. We divided a jet into two distinct zones, the inner and outer regions, depending on the importance of the gravitational effects. One of such effects is that the photons emitted around a black hole are “scattered” into a larger angle. In other words, a distant observer cannot see the innermost portion of the jet (to within a critical radius  $r_c$ ). Physically, photons are of  $q \ll a$  ( $k \approx 1$ ) for  $r < r_c$ . Under these conditions eq. (5) can be solved analytically for approaching jets. Substituting  $r$  with  $1/y$  in the equation, we have

$$\int_0^{y_j} \frac{dy}{\sqrt{1 + a^2 y^2 + 2a^2 y^3}} \approx \frac{1}{r_c} = \frac{1}{a} \ln \left| \tan \left( \frac{\theta_{\text{obs}}}{2} + \frac{\pi}{4} \right) \right| \quad (18)$$

for Kerr black holes, and  $r_c = 1/\theta_{\text{obs}}$  for Schwarzschild black holes, where  $\theta_{\text{obs}}$  defines a critical viewing angle (with respect to the jet axis). Fig 1. shows the results graphically. It is interesting to note that since we are probably looking down the jet in a BL Lac object we would not be able to probe its inner most region. For  $q \rightarrow 0$ , it follows from eqs (5) and (6) that

$$\epsilon_* = \frac{1}{u^t - u^r R_0^{1/2}/\Delta} \quad (19)$$

where  $R_0 = (r_c^2 + a^2)^2 - a^2 \Delta$ , and  $r_c$  is given by eq (18). This is the cutoff photon energy for the inner region.

In the outer region, the gravitational effects are weak and the special relativistic effects are dominant in determining line profiles. Ignoring the general relativistic effects,  $R$  becomes  $R = r^4 - r^2 q^2$  in eq (6) and eq (5) can be solved analytically

$$\frac{q}{r_j} = \sin \theta_{\text{obs}}, \quad \text{and} \quad \epsilon_* \approx \frac{1}{\Gamma(1 - v^r \cos \theta_{\text{obs}})} \equiv \mathcal{D}, \quad (20)$$

where  $v^r$  is the radial velocity of the jets. This is the well-known Doppler shift formula.

For receding jets, on the other hand, there is no  $q$  cut-off (see Figs 4 and 5) with exception of the event horizon. Therefore, the receding jets might allow us to probe deeper into the vicinity of a black hole. For both stellar-mass black holes and AGN, however, the innermost region of a receding jet is likely obscured by the accretion disk, unless the system is viewed nearly edge on. Besides, Doppler de-boosting makes the receding jet much fainter than the approaching jet.

### 3.1. Photon Trajectories

We then derived numerically photon trajectories around a maximally rotating black hole. For approaching jets, the results are shown in Figures 2 and 3 for two jet velocity profiles. The two cases are quite similar. Specifically, the results clearly show a cutoff in  $q$ ; the critical radius ( $r_c$  derived is in rough agreement with our crude estimation (see eq. 18). In the outer region, we see that  $q \propto r_j$ , which again agrees with our analytic results [see eq. (20)]. Fig. 2b shows that that  $x$  is a single-valued function of  $r$  for small viewing angles but becomes double-valued for large viewing angles. This is very important for evaluating the integral in eq. 9.

For receding jets, the photon trajectories are more complicated. In this case, there are actually two possible trajectories for a given photon (see Figures 4 and 5). In other words, the photons emitted with the same energy from the same location could be observed at different times because of the different trajectories they take. This is purely a general relativistic effect. We believe that the effect might become observable if the detectors have high enough timing resolution (Yuan & Wang 2000, in preparation). We also note that the intersection points in figures 4a and 5a indicate that the photons with the same  $q$  at the same location  $r_j$  may even be observed at two different viewing angles.

### 3.2. Emission Line Profiles

The profile of an emission line is clearly affected both by the general and special relativistic effects, which include light bending, gravitational redshift, and Doppler effects. Moreover, it also depends on the emissivity law and velocity distribution of the jet.

#### 3.2.1 Dependence on Viewing Angles

We computed line profiles for different viewing angles, and the results are shown in the Figures 6, 7 and 8. In general, the profiles are quite different from those of the emission lines originating in the accretion disk (Fabian et al 1989, Laor 1991, Kojima 1991, Matt et al 1993, Cadez, Fanton & Calvani 1998, Paniel & Bromley 1998, Hartnoll & Blackman 1999).

For approaching jets around a maximally rotating hole ( $a = 0.998$ ), the line profile is singly peaked for small viewing angles. The position of the peak (Peak I) is simply determined by Doppler blueshift. Toward lower energies, the line is broadened to form a red tail due to gravitational

redshift. As the viewing angle increases, the line profile becomes more complicated. It is in general similar to that of emission lines from a single ring surrounding the black hole (Gerbal & Pelat 1981, Fang & Deng 1982, Zhang, Xiang & Lu 1985), but the two cases are different in nature. The profile is now doubly peaked, with the second peak (Peak II) caused by the combination of gravitational light bending and Doppler effects in the inner region of the jet. More specifically, the photons emitted with a viewing angle  $\theta_0$  less than  $\theta_{\text{obs}}$  would not arrive at a distant observer in the absence of light bending but would if they are scattered into a larger angle  $\theta_0 + \Delta\theta$ , which is equal to  $\theta_{\text{obs}}$ . Now, the energy of the photons are  $\mathcal{D}_0\nu_0/(1+z)$ , which is greater than  $\mathcal{D}_{\text{obs}}\nu_0/(1+z)$  (without light bending), where  $z$  is the gravitational redshift, and  $\mathcal{D}_0 = 1/\Gamma(1 - \beta \cos \theta_0)$ . This is the origin of a doubly-peaked line profile. Given that the gravitational effects become weaker along the jet farther away from the black hole, it is clear that Peak I (pure Doppler peak) is mostly associated with the photons emitted in the outer region while Peak II with the inner region. Quantitatively, the position of Peak II is derived from  $dx/dr = 0$  (see eq. (4)), it follows from equation (9),

$$\frac{du^t}{dr} - \left( \frac{R^{1/2}}{\Delta} \right) \frac{du^r}{dr} = \Xi, \quad (21)$$

where

$$\Xi = \frac{u^r R^{1/2}}{\Delta} \left\{ \frac{2r(r^2 + a^2)}{R} - (r-1) \left[ \frac{a^2 + q^2}{R} + \frac{2}{\Delta} \right] \right\}. \quad (22)$$

Note that the equations can be much simplified for the case of jets with constant velocity. Combining equations (3) and (21), we can quantify the dividing line ( $r_{\text{II}}$ ) between the inner and outer regions. As an example, we show the results in Fig. 9 for the case of  $\theta_{\text{obs}} = 30^\circ$ . The position of Peak II is then given by  $\epsilon_*^{\text{II}} = 1/[u^t - u^r R^{1/2}/\Delta]$ , which is computed at  $r_{\text{II}}$ .

Because  $x$  is a double-valued function of  $r$  for large viewing angles, the observed photons with the same energy may originate from different physical locations. We computed the time-averaged flux for each component. The individual components are also shown in figures 6, 7, and 8 in dotted lines. A more detailed study of the relationship between the two components, such as time lags, is beyond the scope of this investigation.

For receding jets, the line profile is also composed of two components due to two different photon trajectories. At small viewing angles, because the two trajectories are similar, as shown in figures 4 and 5, the line profile is singly peaked. As the viewing angle increases, the difference in the photon trajectories becomes more prominent, which results in a very complicated line profile, as shown in the bottom panels of Fig. 6. The profile now contains four distinct peaks!

### 3.2.2 Dependence on Black Hole Spin

We illustrate the dependence of line profiles on black hole spin by comparing figures 6 and 7, which show the results for the cases of an extreme Kerr black hole and a Schwarzschild black hole, respectively. In the latter case, the profile of an emission line from approaching jets is *always* singly peaked for any viewing angles. The difference

between the two cases can be attributed to our explicit assumption about the starting position of the jets, i.e., at the marginally stable orbit  $r_{\text{ms}}$ . In this context, the inner region of the jets extends closer to a more rapidly rotating black hole, and thus the gravitational effects are stronger. To quantify the discussion, we plotted three important quantities,  $r_{\text{ms}}$ ,  $r_c$ , and  $r_{\text{II}}$ , as a function of black hole spin in Fig. 9. Since the critical radius  $r_c$  is strongly dependent of the viewing angle, we only show a case where the viewing angle is  $30^\circ$ . It is clear that for Schwarzschild black holes  $r_{\text{II}}$  is always less than  $r_{\text{ms}}$  and thus Peak II never forms.

For receding jets, however, the line profile for the case of Schwarzschild black holes is quite similar to that for the case of extreme Kerr black holes. The reason is simple: there is no critical radius ( $r_{\text{II}}$ ) involved here. The rotation of black holes only strengthens the gravitational effects.

### 3.2.3 Dependence on Jet Velocity Profile

We also investigated the dependence of line profiles on jet velocity profile. Comparing the two cases shown in figures 6 and 8, we see quite similar results. There are, however, some differences worth noting. First, there is a discontinuity in the line profiles for cases where a jet has a constant velocity, but none where the jet has an accelerating velocity profile. This is caused by the boundary conditions imposed at the starting point of the jet. The reason is simple: the Doppler effect (dominates over redshift) blueshifts the line at the starting point if the jet has constant velocity. Second, the line profiles are steeper on the red side for cases where a jet has a constant velocity, while they are steeper on the blue side where the jet has an accelerating velocity profile. In the latter cases, continuous acceleration leads to a continuous superimposition of different Doppler shifts, which makes the blue side steeper.

We further explored the parameter space to investigate in detail how the line profiles depend on the accelerating factor  $\gamma$ . In Fig. 10, we summarize the results for different  $\gamma$  values and for both approaching and receding jets. It is clear that the line profiles become markedly different at large  $\gamma$  for approaching jets and they are not nearly as sensitive to  $\gamma$  for receding jets.

### 3.2.4 Dependence on Emissivity Law

Similarly, we studied the dependence of the line profiles on the power-law index ( $m$ ) of the assumed emissivity law for the jets. The results are shown in Fig. 11. As  $m$  increases, the inner region of the jets contributes more and more to the line emission. Therefore, we expect that Peak I becomes weaker and weaker and eventually disappear at very large  $m$ ; this is indeed the case. Given that we know little about the emissivity law of astrophysical jets, we chose to cover a large enough parameter space for completeness.

## 4. CONCLUDING REMARKS

In this work, we conducted a detailed study of the profile of an emission line from both approaching and receding jets. The combinations of strong gravitational effects (including gravitational redshift and gravitational light bending) and Doppler effects can significantly alter the intrinsic

profile of the line. We found that the observed line profiles are also dependent of such factors as the viewing angle, the velocity profile of the jets, and the emissivity law of the jets. We summarize our main results as follows:

- For approaching jets, the emission line is predominantly Doppler blueshifted at small viewing angles. The line profile is singly peaked and is broadened toward lower energies due to gravitational redshift. At sufficiently large viewing angles, however, the line profile becomes doubly peaked, with the second (higher) peak caused by gravitational light bending. For receding jets, the line profile is even more complicated due to different possible photon trajectories. It can have four peaks.
- We quantified the boundary between the inner and outer regions of a jet with which the two peaks in the line profiles are associated for approaching jets.
- We derived a critical radius within which approaching jets become unobservable. This radius increases as the viewing angle decreases. Therefore, it might be difficult to probe the innermost region of the jets in a BL Lac object. Such a constraint does not exist for receding jets.
- We found that the line profile is sensitive to the intrinsic properties of a black hole jet system, such as the spin of the black hole, the Lorentz factor of the jets, the velocity profile of the jets, and the emissivity law of the jets, as well as to external factors such as the viewing angle.

Observationally, although evidence exists for the presence of emission lines from jets both in Galactic black hole systems and AGN, the quality of data is not sufficient for obtaining the line profiles. Therefore, applying our results to observational data is still difficult. Besides, our study makes several critical assumptions about the properties of jets, such as their velocity profile and emissivity law, which are not understood. This makes direct comparisons with observations even harder. Fortunately, new X-ray missions, such as *Chandra* and *XMM*, now carry instruments that provide unprecedented spectral resolution and sensitivity. Hopefully, the new data is of sufficiently good quality that allows us to identify emission lines from jets in Galactic black hole systems and AGN, based on this work. A detailed characterization of such lines might lead to a determination of such fundamental properties as the angular momentum of the black holes and perhaps shed significant light on the properties of the jets themselves.

The authors are very grateful to Wei Cui, the referee, for his a large number of very detail and helpful comments to clarify several points of this paper. Especially on the generalities of the present calculations, and the emissivity law assumption. We also thank his suggestions supplementing the calculations for the receding jet. We thank F.J. Lu for his careful reading of the manuscript. J.M.W. is grateful to Durouchoux for his useful comments and discussions during his visiting IHEP. The useful suggestions from M. Calvani are greatly acknowledged. The authors would like to thank T.P. Li, J.F. Lu and T.G. Wang, S.J. Xue, and J.L. Qu for the interesting discussions. J.M.W. is supported by 'Hundred Talents Program of CAS'. This research is partially supported by NSFC.

#### REFERENCES

- Ames, W.L. & Thorne, K.S., 1968, *ApJ*, 151, 659  
 Bardeen, J.M., Press, W.H., & Teukolsky, S.L., 1972, *ApJ*, 178, 347  
 Blackman, E.G., 1999, *MNRAS*, 306, L25  
 Cadez, A., Fanton, C. & Calvani, M., 1998, *New A.*, 3, 647  
 Carter, B., 1968, *Phys. Rev.*, 174, 1559  
 Cui, W., Chen, W. & Zhang, S.N., 1999, *astro-ph/9909023*  
 Cunningham, C.T., & Bardeen, J.M., 1973, *ApJ*, 183, 237  
 Fabian, A.C. & Rees, M.J., 1979, *MNRAS*, 187, 13  
 Fabian, A.C., Rees, M.J., Stella, L & White, E., 1989, *MNRAS*, 238, 729  
 Fabian, A.C., et al , 1995, *MNRAS*, 277, L11  
 Fang, L.Z., & Deng, T.R., 1982, *Acta Phys. Sinica*, 31, 109  
 Hartnoll, S.A. & Blackman, E.G., 1999, *astro-ph/9908275*  
 Gerbal, D. & Pelat, D., 1981, *A&A*, 95, 18  
 Gerlach, U.H., 1971, *ApJ*, 168, 481  
 Kojima, Y., 1991, *MNRAS*, 250, 629  
 Koide, S., Meimer, D.L., Shibata, K., Kudoh, T, *astro-ph/9907435*  
 Laor, A., 1991, *ApJ*, 376, 90  
 Matt, G., Perola, G.C., Stella, L., 1993, *A&A*, 267, 643  
 Margon, B., 1984, *ARA&A*, 22, 507  
 Margon, B., et al, 1979, *ApJ*, 230, L41  
 Misner, C.W., Thorne, K.S., & Wheeler, J.A., *Gravitation*, 1970, W.H. Freeman and Company, San Francisco  
 Misra, 1999, *astro-ph/9912178*  
 Pariev, V.I. & Bromley, B.C., 1998, *ApJ*, 508, 590  
 Reynolds, C. S., 1997, *MNRAS*, 286, 513  
 Reynolds, C.S., 1999, *ApJ*, in press  
 Reynolds, C.S. & Begelman, M.C., 1997, *ApJ*, 488, 109  
 Tanaka, H, et al, 1995, *Nature*, 375, 659  
 Thorne, K.S., 1967, in *High Energy Astrophysics*, Vol 3, ed. C. Dewitt, E. Schatzman & P. Véron (New York: Gordon & Breach)  
 Yaqoob, T., George, I.M., Nandra, K., Turner, T.J., Zobair, S. & Serlemitsos, P.J., 1999, *ApJ*, 525, L9  
 Yaqoob, T., George, I.M., Turner, T.J., Nandra, K., Ptak, A., Serlemitsos, P.J., 1998, *ApJ*, 505, L87  
 Zhang, J.L., Xiang, S.P., & Lu, J.F., 1985, *Ap&SS*, 113, 181

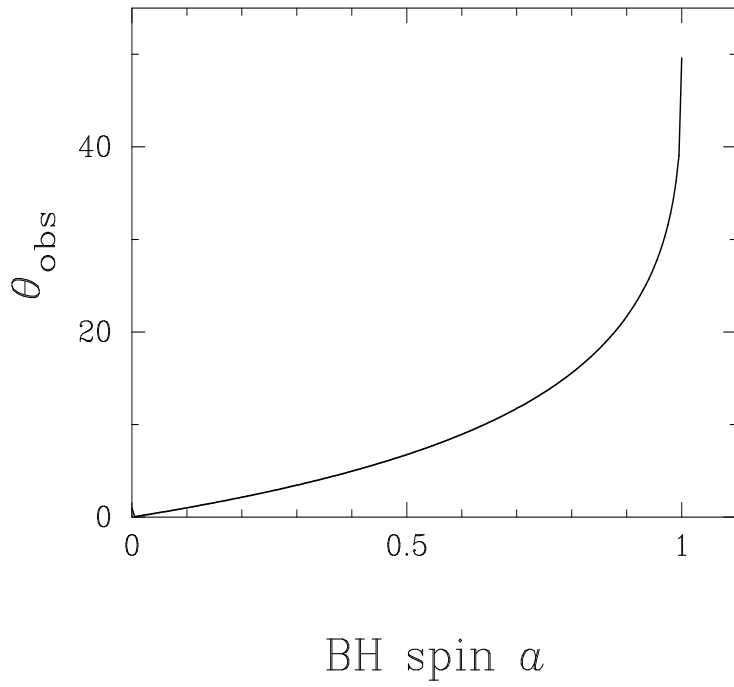


FIG. 1.— The relation between spin of black hole and viewing angle. This constraints the observable region of the approaching jet.

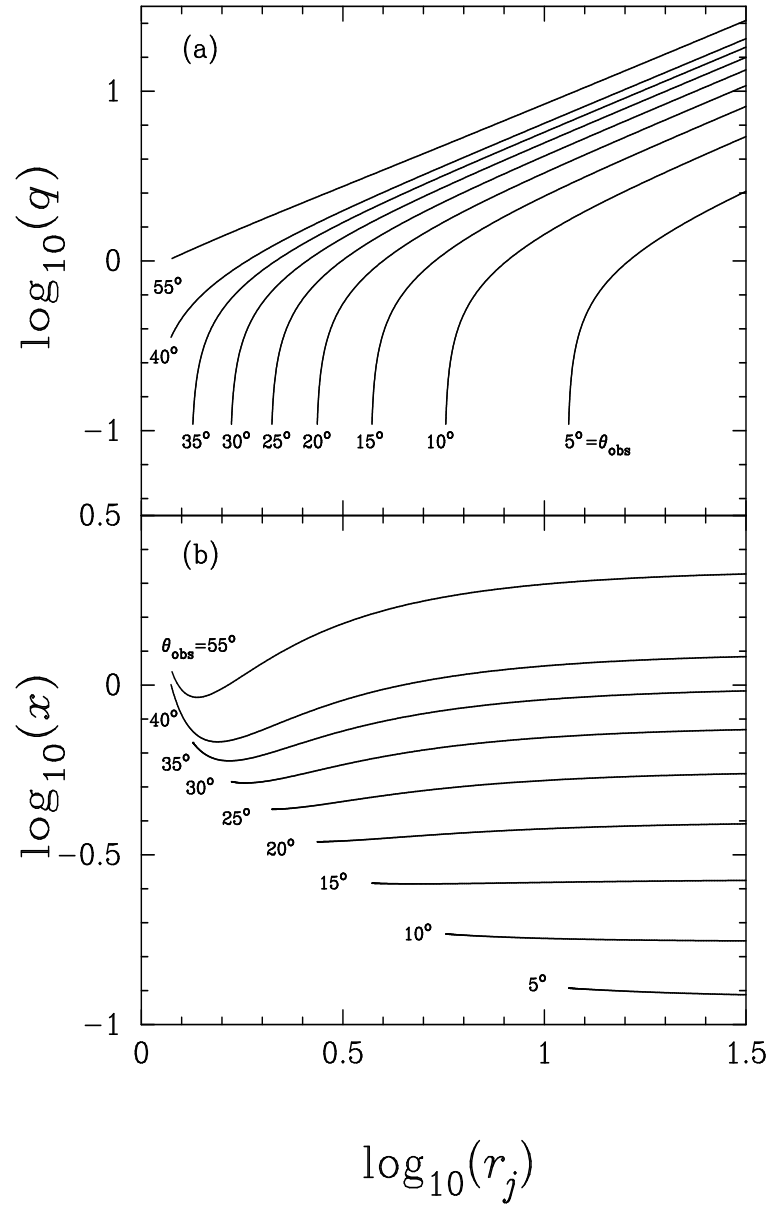


FIG. 2.— The solution of trajectory equation for the case of the approaching jet with constant Lorentz factor  $\Gamma_0 = 5$  to the observer and  $a = 0.998$ . It can be found that the solution of  $q$  is strongly dependent on the viewing angle of the observer, especially the cutoff of  $q$ . This can be deduced from equation (16). The observer can not see the region within the critical distance  $r_c$ . The parameter  $x$  is a double-valued function of  $r$  when an observer has above certain viewing angle, but a single-valued function of  $r$  for small viewing angle.

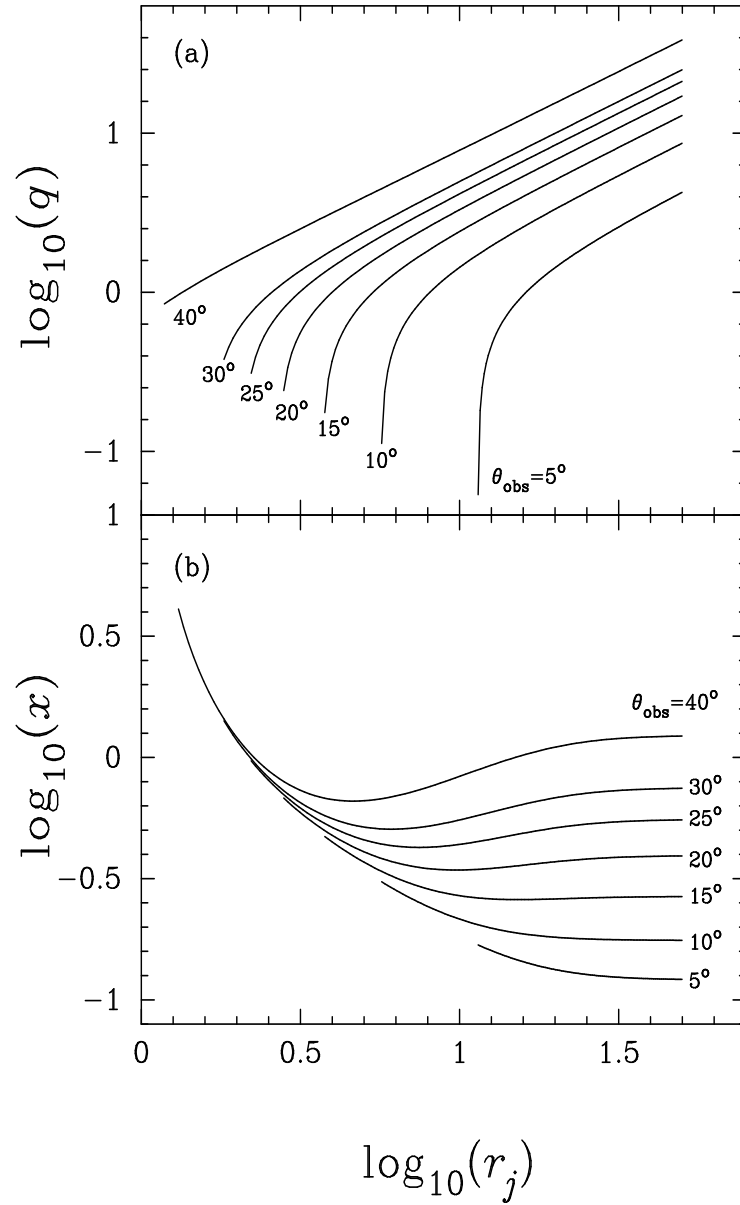


FIG. 3.— The solution of trajectory equation for the case of approaching jet to the observer, but the velocity distribution is described by equation (7). The final Lorentz factor  $\Gamma_0 = 5$ ,  $a = 0.998$  and the acceleration factor  $\gamma = 7.5 \times 10^{-2}$ . Although the properties of  $q$  value is the same with the case of constant velocity, the value of  $x$  is different.



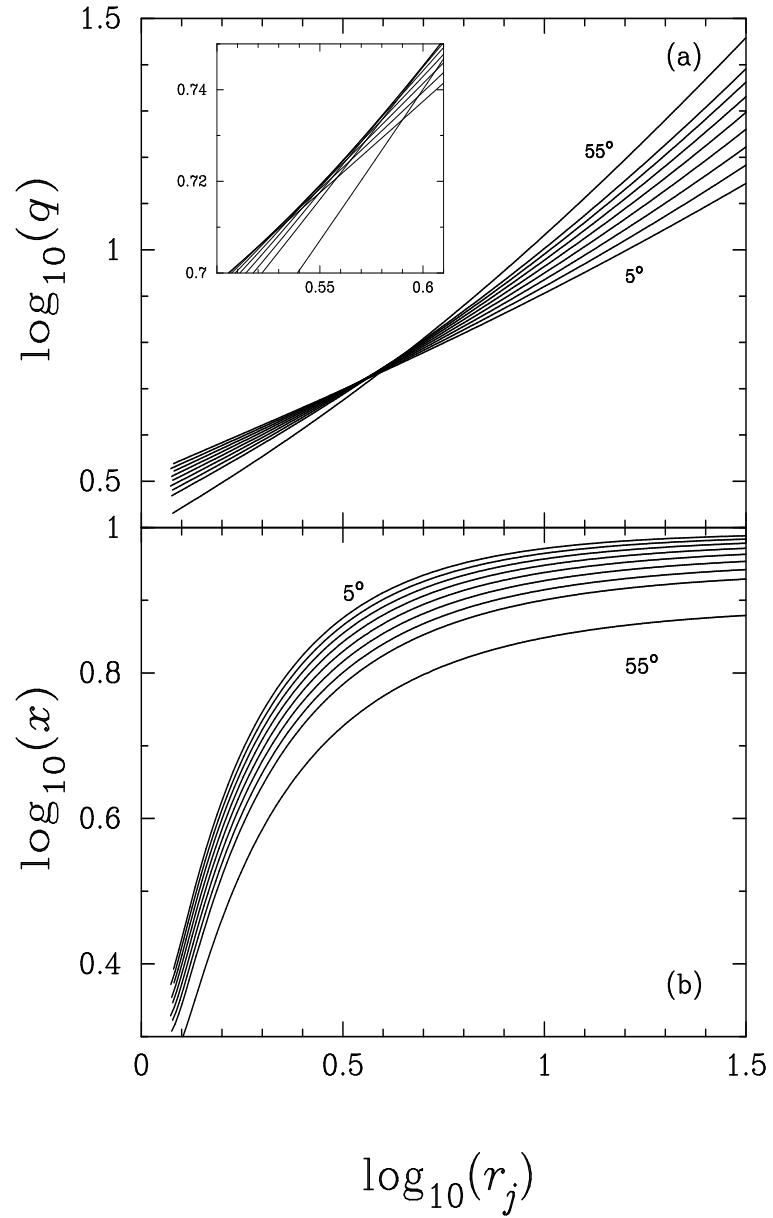


FIG. 4.— The solution of trajectory equation for the case of the receding jet to the observer. This figure corresponds to the first kind trajectory of photons, namely without  $\theta$ -turning point. It is seen that  $x$  changes singly with  $r_j$ . We take  $\Gamma_0 = 5$ .

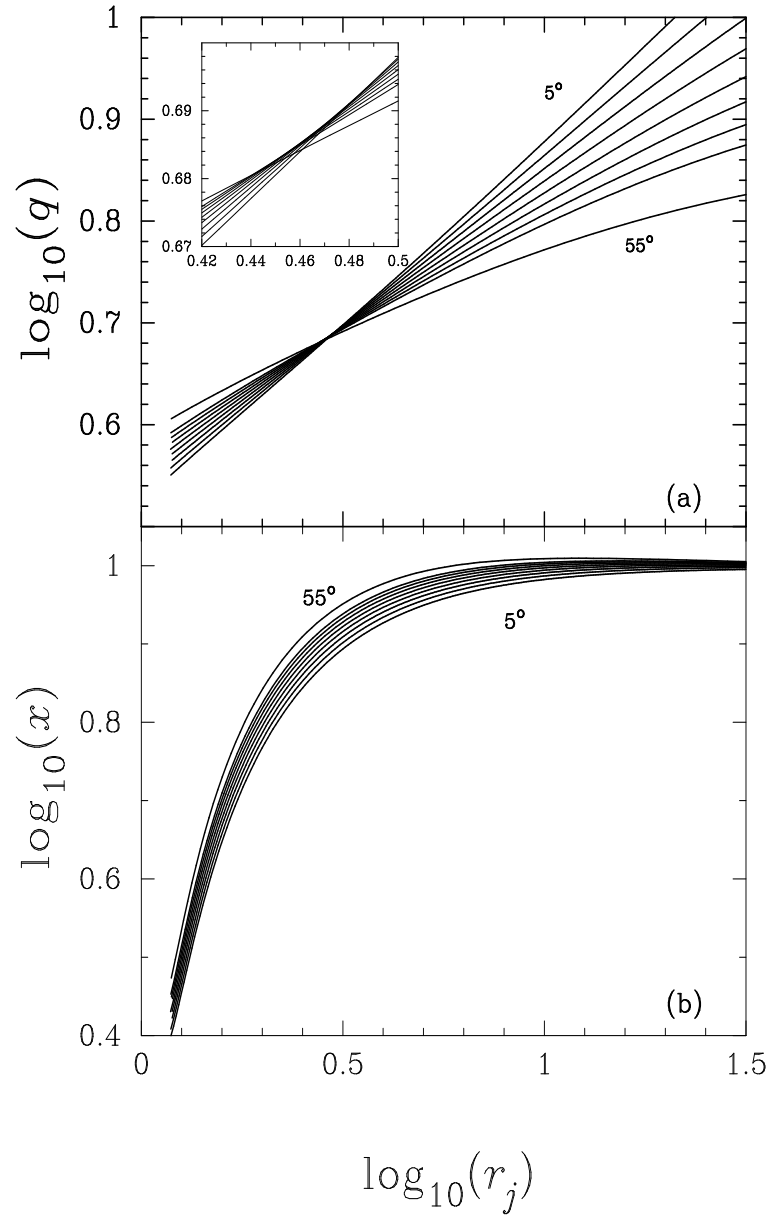


FIG. 5.— The solution of trajectory equation for the case of the receding jet to the observer. This figure represents the case of the second kind trajectory of photons, i.e. with  $\theta$ -turning point.

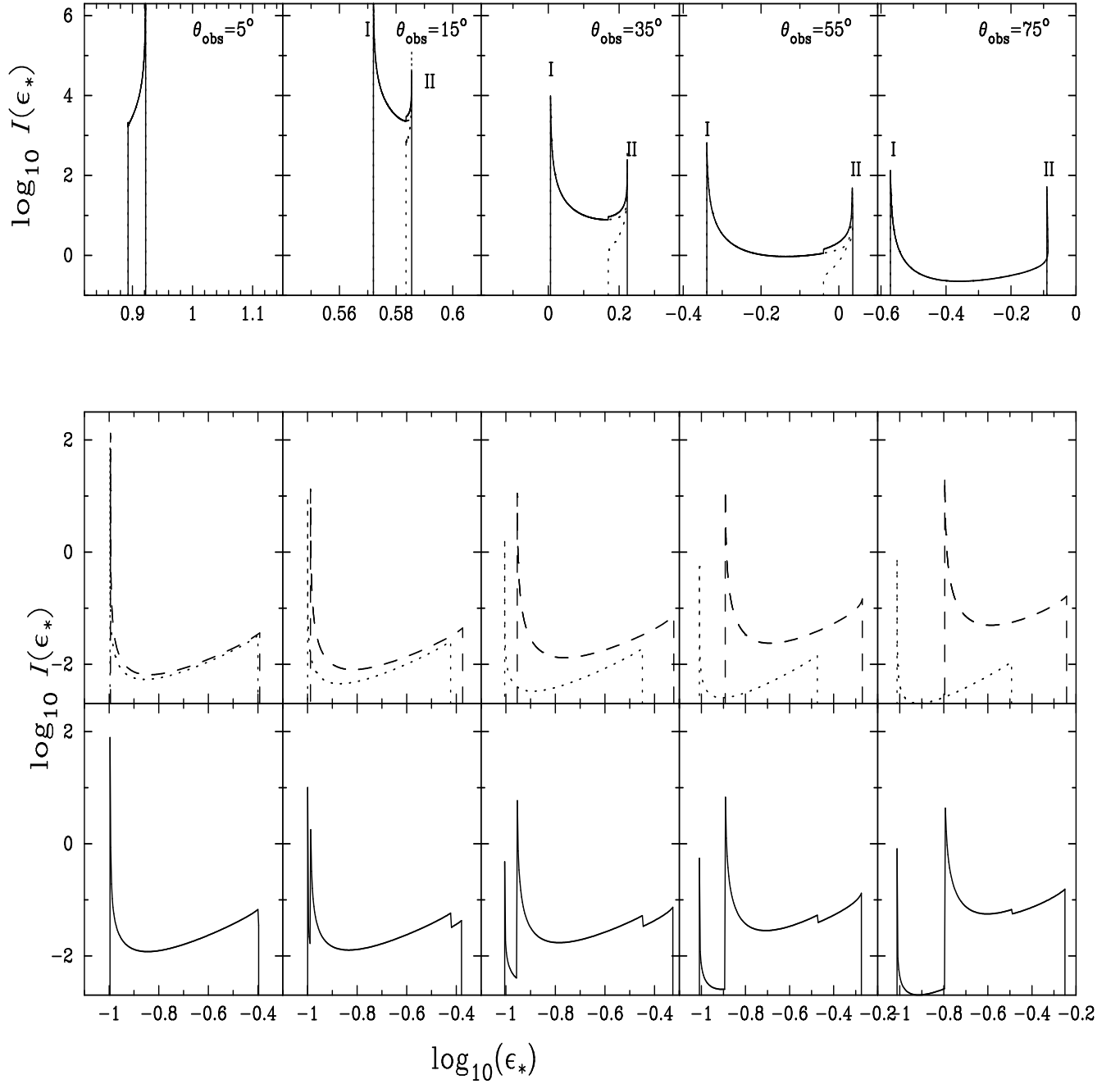


FIG. 6.— The received profile (in arbitrary unit) of an emission line from relativistic jet at infinity. The parameters of the model are: the jet moves with a constant Lorentz factor  $\Gamma_0 = 5$ , index of emissivity law  $m = 0.5$  and the spin  $a = 0.998$ . The upper panels are that from the approaching jet. The middle ones are the two components from receding jet. The bottom panels are the total profiles from the receding jet. The strong dependence of received profile on viewing angle is clearly shown. It is found that there two components: the dotted lines originates from two different region of outflow. The upper dotted line represents the emission from outer part of outflow whereas the lower dotted line does that from more inner region. The solid line does the sum of the two components observed as time averaged flux. The two peaks are marked by I and II, which originate from the Doppler effect in the outer and inner region, respectively.

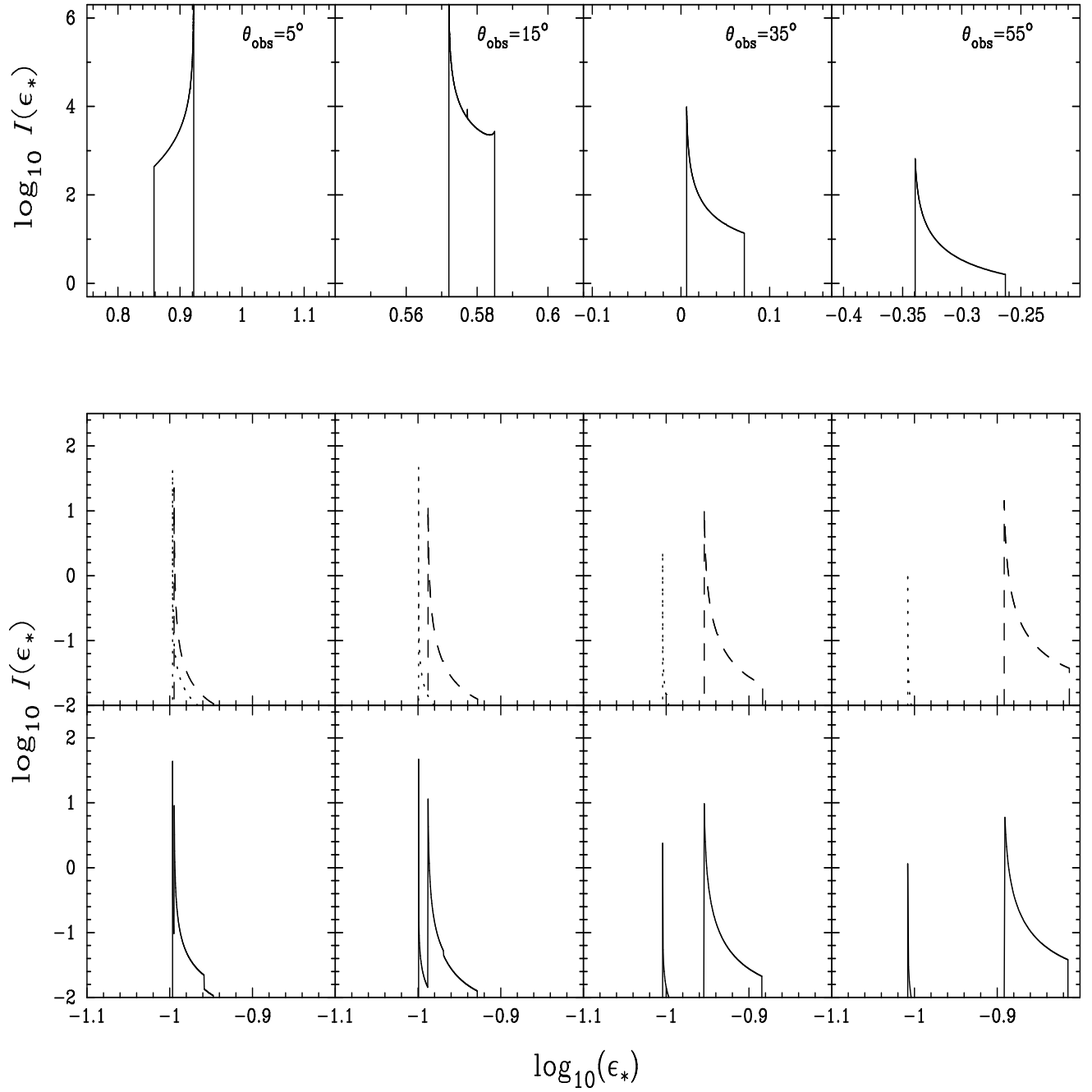


FIG. 7.— The received profile (in arbitrary unit) of an emission line from relativistic jet at infinity. The parameters are taken as same with the Fig. 6, but the spin  $a = 0.0$ .

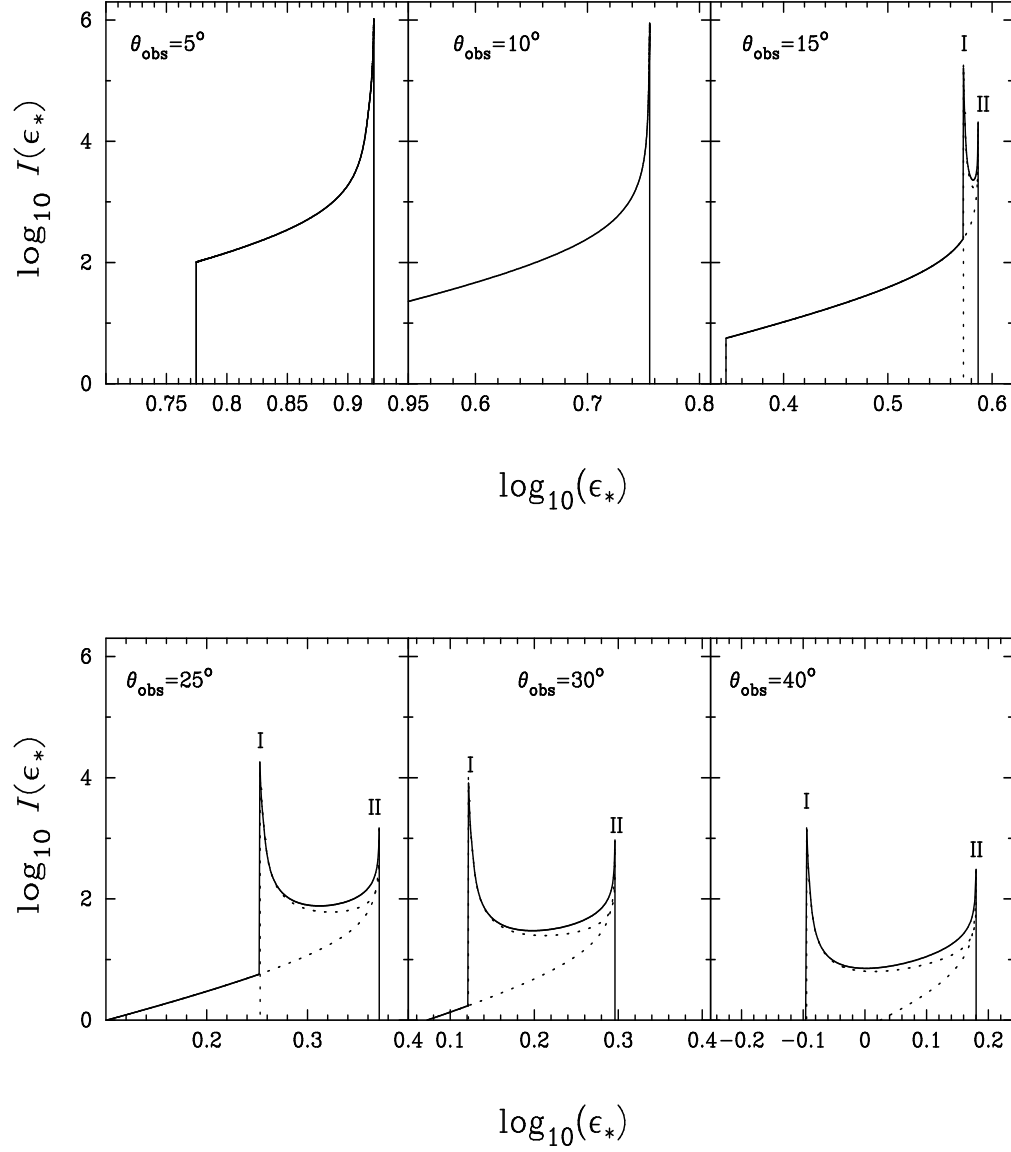


FIG. 8.— The received profile (in arbitrary unit) of an emission line from relativistic jet at infinity. The parameters of the model are: the accelerating factor  $\gamma = 7.5 \times 10^{-2}$ , the final Lorentz factor  $\Gamma_0 = 5$ , index of emissivity law  $m = 0.5$  and the spin  $a = 0.999$ .

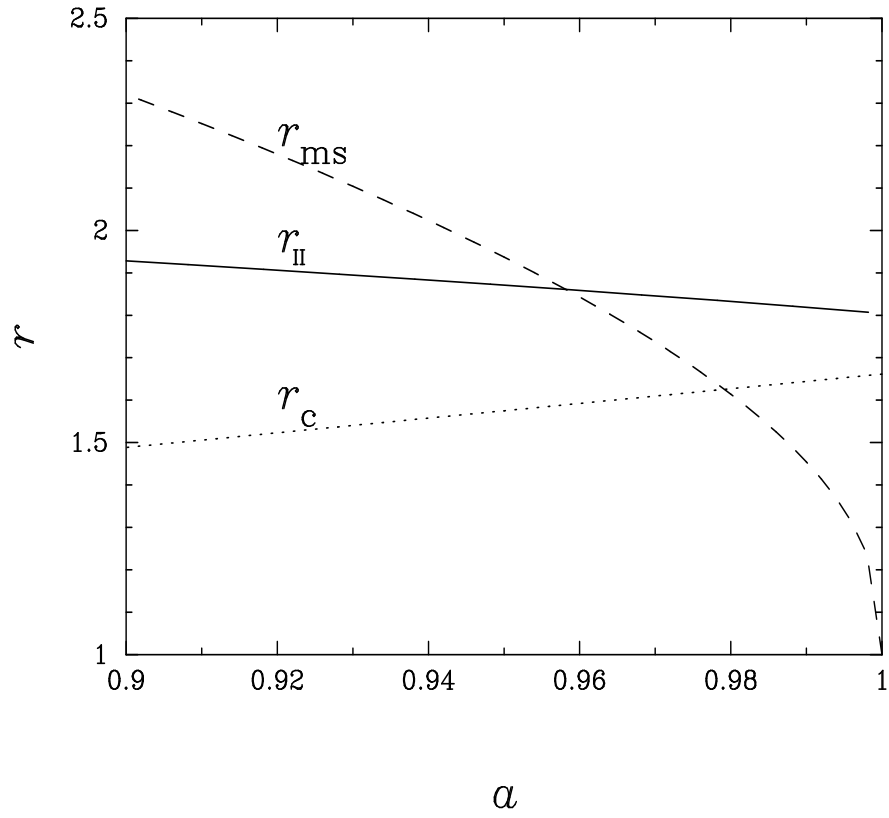


FIG. 9.— The parameter space for the Peak II.  $r_{ms}$  is the dashed line,  $r_c$  is the critical line by equation (16), and the dotted line is the location producing the Peak II. This figure shows the important role of spin parameter  $a$  in the formation of Peak II. We take the viewing angle  $\theta_{obs} = 30^\circ$ .

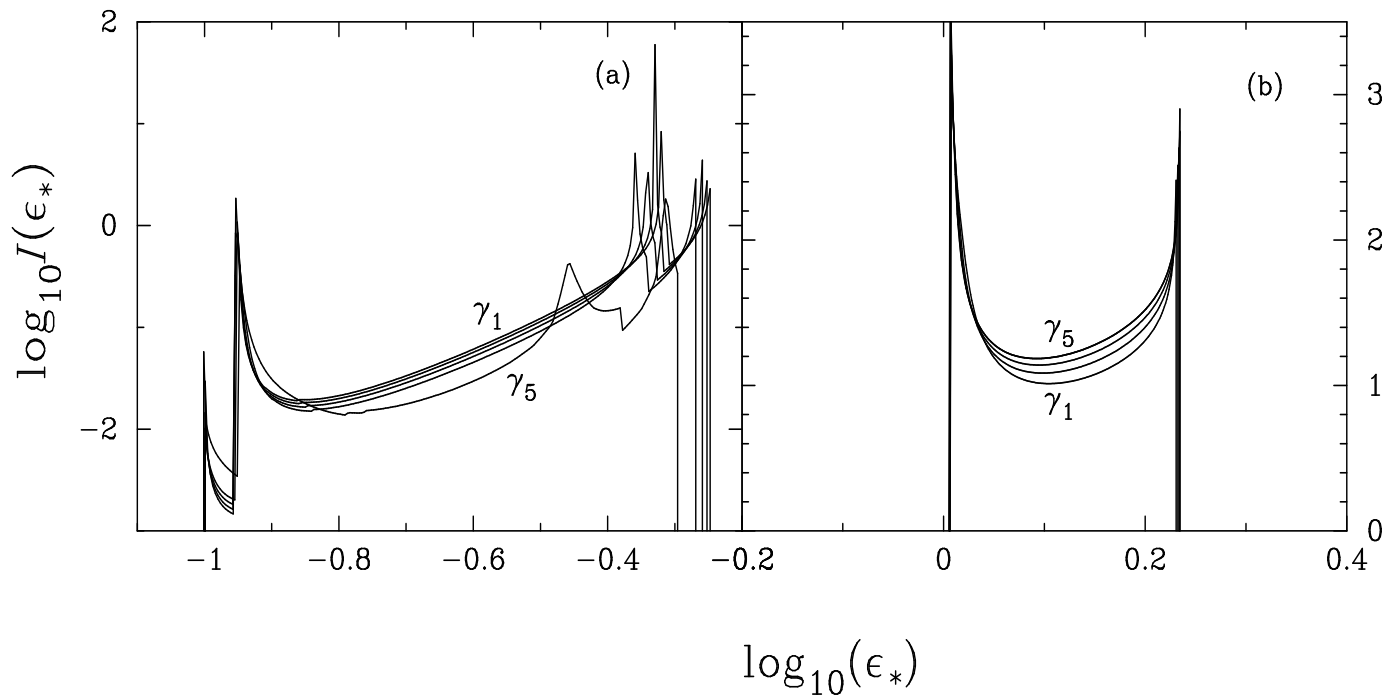


FIG. 10.— These figures are used to test the dependence of observed profile on the accelerating factor  $\gamma$ . We  $\theta = 35^\circ$ ,  $a = 0.998$ ,  $m = 0.5$  and  $\Gamma_0 = 5$ . The accelerating factor  $\gamma$  is taken to be  $(6.0, 7.5, 10, 15) \times 10^{-2}$ . The line for  $\gamma = 1$  has been plotted and labeled by  $\gamma_5$ . We can see that the profiles for approaching and receding jet have the different dependence on  $\gamma$ . The profile from approaching jet for  $\gamma_4 = 0.15$  is overlapped by that of  $\gamma_5 = 1$ .

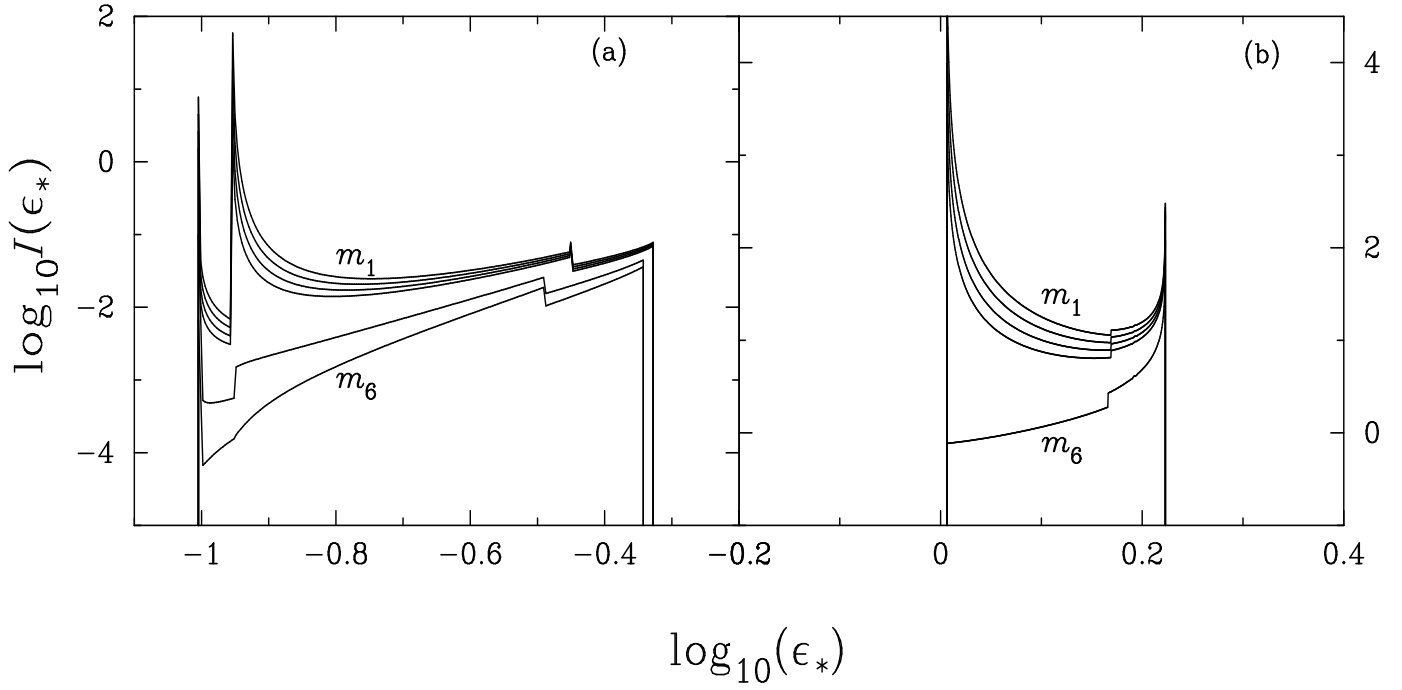


FIG. 11.— These figures are used to test the dependence of observed profile on the index  $m$  of the emissivity law. We  $\theta = 35^\circ$ ,  $a = 0.998$ , and  $\Gamma_0 = 5$ . The index  $m$  is taken to be (0.1, 0.3, 0.5, 0.7). The line labeled by  $m_6$  is the profile for  $m_6 = 3$ . The case for  $m_5 = 2$  is overlapped by that of  $m_6 = 3$ . For such a large  $m$  the one peak disappears.